Title

Centrifuge Modeling Methodology for Energy Pile Pullout from Saturated Soft Clay

Journal

Geotechnical Testing Journal, 45(2)

ISSN

0149-6115

Authors

Ghaaowd, Ismaail

McCartney, John S

Publication Date

2022-03-01

DOI

10.1520/gtj20210062

Peer reviewed

Centrifuge Modeling Methodology for Energy Pile Pullout from Saturated Soft Clay

Ismaail Ghaaowd, Ph.D.

Research Engineer II, Turner-Fairbank Highway Research Center, High-Performance Technologies, Inc., 13800 Coppermine Rd., Herndon, VA 20171; ighaaowd@hptech-inc.com

John S. McCartney, Ph.D., P.E., F.ASCE

Professor and Chair, Dept. of Structural Engineering, Univ. of California San Diego, 9500 Gilman Dr., La Jolla, CA 92093-0085; mccartney@ucsd.edu

ABSTRACT: This paper describes a test setup and methodology for centrifuge modeling of energy pile pullout from saturated soft clay, with the goal of understanding how pile heating improves the interface shear strength through thermal consolidation. A kaolinite clay layer was first consolidated outside the centrifuge within a cylindrical container having an inner diameter of 551 mm using a hydraulic piston to reach a thickness of 220-240 mm then permitted to equilibrate in the centrifuge under 50 g. An aluminum energy pile having a model-scale diameter of 25 mm and length of 255 m was then installed at a constant displacement rate through the clay layer and embedded into an underlying sand layer. An electrical resistance heater within the pile was used to heat the soil-pile interface to a target temperature and thermocouples and pore water pressure transducers in the clay layer were used to track the coupled heat transfer and water flow processes. Detailed results are reported from a baseline test on an unheated pile and from a test on a pile where pullout was performed after heating the pile from 20 to 65 °C and cooling back to 20 °C with no head restraint. The pullout capacity of the heated energy pile was 1.43 times greater than that of the unheated energy pile. Insights into the increase in capacity were gained from undrained shear strength profiles in the clay layers measured using push-pull T-bar penetration tests performed after pullout.

KEYWORDS: Energy piles, soft clay, pullout, centrifuge modeling, thermal consolidation

INTRODUCTION

Because of their relatively low undrained shear strength and high compressibility, soft clay deposits routinely pose challenges to geotechnical engineers interested in improving the axial load-carrying capacity of deep foundations or piles. Beyond increasing the dimensions or mass of piles, several techniques have been used to increase the pullout capacity of piles by enhancing the mechanical behavior of the surrounding soft clay layer, including preconsolidation with a surcharge or vacuum loading, installation of vertical drains, or electro-osmosis (Nicholson 2015). While these soil improvement techniques have been shown to work well for soft clay deposits on land, they may be difficult to implement in offshore clay deposits. Accordingly, increasing the pullout capacity of offshore piles in soft clays used as anchors for floating structures is particularly important to avoid having to install additional piles to meet the required anchorage support. A promising soil improvement technique may be to convert deep foundation into an energy pile that can be used to strategically heat the surrounding soil and improve its mechanical behavior via thermal consolidation. Thermal consolidation has been used successfully to densify soft clays using arrays of geothermal heat exchangers (Bergenstahl et al. 1994) or thermal drains (Abuel-Naga et al. 2006; Pothiraksanon et al. 2010; Artidteang et al. 2011; Salager et al. 2012), but has not yet been investigated for energy piles in soft clays. While several studies have investigated the behavior of energy piles in soft clays (Ng et al. 2014; Yazdani et al. 2019, 2020), they considered temperature ranges representative of heat exchange applications (maximum temperatures of 34-38 °C) that are lower than those necessary for thermal improvement (e.g., temperatures of 60-80 °C were used by Bergenstahl et al. 1994).

This study proposes a thermal soil improvement concept that builds upon but also deviates from recent research on energy piles, where closed-loop fluid circulation pipes are embedded into

a reinforced concrete pile to convert it to a geothermal heat exchanger (Brandl 2006). Most studies on energy piles have focused on the behavior of energy piles in relatively stiff soil deposits with downward axial loading under temperatures ranging from 5 to 40 °C (e.g., Brandl 2006; Laloui et al. 2006; Bourne-Webb et al. 2009; Murphy et al. 2015; Murphy and McCartney 2015; McCartney and Murphy 2017). When simulating energy piles in stiff soil deposits it is often assumed that the soil is thermo-elastic (e.g., Laloui et al. 2006). While nonlinear interface stress-displacement curves have been considered in load-transfer analyses (e.g., Knellwolf et al. 2011; Chen and McCartney 2016), these studies did not consider elasto-plastic changes in the stress-displacement curve with temperature associated with thermal consolidation. Different from typical energy pile heat exchange operations, the concept of soil improvement using energy piles proposed in this study is to increase the temperature of the pile by a target increment and maintain this elevated temperature for a certain time before cooling back to ambient temperature after thermal consolidation is complete. An electrical or chemical heating element may be used in the pile in the case that heat exchange tubing cannot be installed. The imposed change in temperature should be significant enough to lead to appreciable thermal consolidation (i.e., 60 to 80 °C), but not so high as to risk thermal failure where the change in pore water pressure approaches the mean total stress (Houston et al. 1985). This change in temperature of the pile, which is assumed to be uniform with depth based on observations from instrumented energy piles (e.g., Murphy et al. 2015), is expected to result in thermal pressurization and generation of excess pore water pressure due to the differential thermal expansion of the clay particles and water (Campanella and Mitchell 1968). This change in pore water pressure may increase with depth (Uchaipichat and Khalili 2009; Ghaaowd et al. 2017). Ghaaowd et al. (2017) reviewed several studies on undrained heating from the literature and found that the magnitude of excess pore water pressure generation depends on

the plasticity index of the clay as well as the stress state and initial void ratio. As soon as thermally induced excess pore water pressures are generated, water flow will occur away from the heat source (the energy pile) and the excess pore water pressure will decrease with time until returning to hydrostatic conditions. Accordingly, fully undrained heating is not expected and depending on the permeability of the soil, the heating process may result in partial drainage where excess pore water pressures dissipate as it is generated and do not reach the magnitudes predicted using approaches like Campanella and Mitchell (1968) or Ghaaowd et al. (2017).

The generation and dissipation of excess pore water pressure in saturated soils is known to be closely coupled with changes in volume, which are in turn coupled with changes in undrained shear strength (e.g., Houston et al. 1995; Samarakoon et al. 2018). Undrained heating of soils leads to elastic thermal expansion (e.g., Uchaipichat and Khalili 2009). Berghenstahl et al. (1994) observed an initial thermal expansion of a normally consolidated clay layer immediately after heating before drainage started to occur. As the thermally-induced excess pore water pressures dissipate, permanent volume changes may occur depending on the stress history of the soil layer. Of greatest interest to this study are normally consolidated soils, which will contract volumetrically during drainage of thermally induced excess pore water pressures, or during drained heating (where the rate of heating is so slow that excess pore water pressures dissipate as soon as they are generated). Attaining this volumetric contraction is the main objective of the thermal soil improvement process. Accordingly, it is important that the increased temperature be maintained until thermo-hydraulic equilibrium is reached and thermal volume changes are stabilized, as premature cooling will reduce the thermally induced excess pore water pressures that drive the thermal improvement process.

A wealth of experience on the volume change of saturated clays during drained heating from element-scale tests has been established in the literature (Baldi et al. 1988; Towhata et al. 1993; Hueckel et al. 1998; Burghignoli et al. 2000; Sultan et al. 2003; Cekerevac et al. 2005; Abuel-Naga et al. 2007a, 2007b; Takai et al. 2016; Samarakoon et al. 2018; Zeinali and Abdelaziz 2021). The studies indicate that normally consolidated clays experience a plastic contractile volumetric strain of approximately 1 to 2% during heating to temperatures up to 90 °C, depending on the clay mineralogy and initial void ratio. While overconsolidated soils will experience excess pore water pressure generation during undrained heating similar to normally consolidated soils, they show a transitional response in volume change during drained heating (Baldi et al. 1988; Vega and McCartney 2015). For example, lightly overconsolidated clays may contract by a smaller amount than normally consolidated clays during drained heating, while heavily overconsolidated clays will expand elastically during drained heating. Accordingly, this thermal improvement technique is most appropriate for normally consolidated and lightly overconsolidated soils. The results from the literature also indicate that after reaching thermo-hydraulic equilibrium, further volumetric contraction may occur during cooling due to elastic contraction, depending on the rate of cooling. In some cases, a partial recovery of thermal strains can occur for fast cooling (e.g., Samarakoon and McCartney 2020). The cumulative decrease in void ratio of the clay following a heating-cooling cycle will lead to an increase in the undrained shear strength of the clay (Houston et al. 1985; Samarakoon et al. 2018). This change in undrained shear strength of the soil surrounding an energy pile will result in a change in ultimate bearing capacity, and for the case of offshore foundations used as anchors it will result in an increase in pullout capacity.

The process of soil improvement using in-situ heating in saturated, normally consolidated clays is expected to be a complex, coupled thermo-hydro-mechanical process. Heat transfer in saturated

soils may be due to a combination of both conduction and convection, as changes in the pore water density with temperature may lead to buoyancy-driven water flow. However, Saviddou (1988) found that for clays with low hydraulic conductivity, heat transfer due to convection will be slower than that due to conduction. Accordingly, this study only considers conductive heat transfer. Generation of excess pore water pressures will lead to flow of water away from the heat source (the pile), leading to time-dependent thermal consolidation (Booker and Savvidou 1985; Zeinali and Abdelaziz 2021). Thermal volumetric contraction will lead to a decrease in hydraulic conductivity, which may slow the improvement process. However, thermal volumetric contraction will also lead to an increase in thermal conductivity, affecting the heat transfer process. The zone of influence of the thermal consolidation process will depend on the applied temperature boundary condition (magnitude and duration) as well as the characteristics of the surrounding soil. But for normally consolidated soils an improvement is expected in the same zone of influence as a change in temperature.

The centrifuge physical modeling methodology developed in this study builds upon previous work on the consideration of temperature effects in soft clays. Maddocks and Savvidou (1984) investigated the heat transfer from a hot cylinder installed in soft saturated clay in a centrifuge test, and observed the generation and dissipation of excess pore water pressure and subsequent thermal consolidation as a function of distance from the cylinder. Ng et al. (2014) used a centrifuge to study the effects of cyclic heating of an aluminum energy pile in soft clay and observed permanent settlement that accumulated with each cycle. Ng et al. (2019) found that heat transfer in clays due to conduction was not affected by the g-level and confirmed the scaling factor for diffusive time of N^2 derived by Saviddou (1988). Stewart and McCartney (2014) and Goode and McCartney (2015) found that centrifuge modeling provides useful information on soil-structure interaction

phenomena and load testing to failure for energy piles that cannot be obtained easily from full-scale testing, and centrifuge test results are useful for validation of numerical simulations. Physical modeling of thermal improvement of soft clays using in-situ heating has not been fully explored and could benefit from further experimental evaluations like those in this study.

This study presents the details of a centrifuge physical modeling methodology developed to assess the impact of a heating-cooling cycle on the pullout capacity of energy piles embedded in soft clay layers. The results from tests on heated and an unheated energy piles in separate soil layers within the geotechnical centrifuge at the University of California San Diego are presented in this study to demonstrate the methodology and typical results. After preparation of a soft clay layer, the energy pile was installed using jacked-in procedures, heated to a constant temperature with an unrestrained head boundary condition, cooled, then pulled out at a constant rate after reaching equilibrium. Preliminary tests on this topic were presented by Ghaaowd and McCartney (2018) and Ghaaowd et al. (2018), albeit with an energy pile having a fixed head boundary condition during heating which may not be representative of offshore piles that act as anchors for floating structures. The fixed head boundary condition in the energy piles considered in these preliminary studies may prevent possible mobilization of side shear stresses along the length of the end-bearing pile during the heating process, which may affect the pullout force-displacement curve. In addition to the load-displacement curves from installation and pullout, data on variations in temperature and pore water pressure generation in the clay layer and measurements of the undrained shear strength profile using a T-bar test are presented to interpret the coupled thermo-hydro-mechanical soil improvement process. The methodology presented in this study may be used to assess the conditions leading to thermal improvement for anchors in normally consolidated

clay layers as part of a pile design process and provide useful information for validation of numerical simulations.

EXPERIMENTAL SETUP

The Actidyne C61-3 geotechnical centrifuge at the University of California San Diego shown in Figure 1 was used in this study. This 50 g-ton geotechnical centrifuge was designed to carry payloads a maximum mass of 500 kg up to 100 g. The specifications of the UCSD geotechnical centrifuge are shown in Table 1. Centrifuge testing uses the concept of geometric similitude to ensure that a model with reduced dimensions will have a similar stress state to a prototype in the field (Kutter 1992). Centrifuge modeling permits careful control of soil layer preparation, dense instrumentation arrays, and parametric evaluations of different key variables that may not be possible in field prototype testing, while ensuring that stress-dependent soil properties and soil-structure interaction mechanisms are captured under a representative stress state. In the case of the centrifuge testing program detailed in this study, all tests were performed at a centrifugal acceleration of 50 g (i.e., N = 50).

An aluminum cylindrical container with an integrated reaction frame was developed for this testing program, with a cross-sectional schematic shown in Figures 2(a) and 2(b). The aluminum container consists of a base plate, a cylindrical tank, and an upper reaction plate where loading motors or a hydraulic piston can be mounted. The base and reaction plates of the container have dimensions of 0.62 m × 0.62 m × 0.05 m, which corresponds to the internal dimensions of the centrifuge basket. The cylindrical tank has an inside diameter of 0.55 m, a wall thickness of 16 mm, and a height of 0.47 m, and was connected to the base plate via four restraining brackets that connect to threaded rods shown in Figure 2(c). The base plate has an “O”-ring groove to provide a water-tight seal. The top reaction plate can be fixed at different locations above the cylindrical

tank using bolts. The reaction plate supports stepper motors for applying axial loads to the energy pile and T-bar, as shown in Figure 2(d). Drainage from the base of the container is permitted using a porous stone connected to a drainage port in the bottom of the base plate. A standpipe was connected to the drainage port that can be connected to a selected port in the container side wall corresponding to a layer of ponded water atop the clay layer to maintain double drainage conditions.

The scale-model energy pile consists of a 25 mm-diameter, 255 mm-long, aluminum split-shell cylinder having a wall thickness of 3.3 mm, as shown in Figure 3. At 50 g, the model pile corresponds to a prototype pile having a diameter of 1.25 m and a length of 12.75 m. The insides of the cylinder halves were instrumented with thermocouples which measure the temperature at the pile wall. Internal strain gages were also installed but did not function well during heating to high temperatures and were not used in this study. This study focused only on the pullout response of the pile so soil-structure interaction mechanisms or the axial rigidity of the pile were not considered. The pile was assumed to act like a rigid body for the pullout analyses, which is a reasonable assumption for a short pile in soft soil. The halves of the split-shell cylinder are held together by screw-on top and bottom caps. To control the pile temperature, a cylindrical 500W Watlow Firerod heating element having a diameter of 12 mm and a length of 200 mm was centralized within the pile. The space between the heating element and the split-shell cylinder was filled with dense Ottawa sand to act as a thermal grout to promote uniform heat exchange. In addition to a K-type thermocouple within the heating element, two additional K-type thermocouples were installed on the inside of the aluminum pile surface. The heating element was connected to a Watlow EZ Zone PM controller to control the temperature during centrifugation, using the output from the thermocouple on the inside surface of the aluminum shell of the pile at

mid-height as the control objective when applying a target temperature. Accordingly, the effects of the thermal grout on heat transfer from the heater to the outer shell of the pile were not considered. The coefficient of thermal expansion of the pile was found to be 24 με/°C, which is close to that of aluminum despite the different components of the pile (steel heating element, sand grout, aluminum shell). The controller was interfaced with LabVIEW on a computer located on the arm of the centrifuge which was remotely accessed from a host computer in the centrifuge control room. The heating element and heat controller had sufficient power to apply temperatures measured at the inside surface of the pile shell as high as 80 °C, although higher temperatures are possible. To minimize heat transfer to the water ponded above the clay surface, the top cap was fabricated from Delrin to provide an insulating effect while still being sufficiently stiff for applying mechanical loads. This top cap design was found to not lead to significant heating of the water on top of the clay surface. The top cap also contained several holes to provide access for the internal instrumentation wires.

A T-bar penetrometer having dimensions shown in Figure 4 was used to perform penetration-extraction tests to measure the undrained shear strength profile in the clay layer using the correlations developed by Stewart and Randolph (1991). The T-bar can be used to measure the intact undrained shear strength during downward penetration, and the disturbed undrained shear strength during extraction, which permits evaluation of the sensitivity of the soil layer. The load applied to the T-bar was only measured at the head of the T-bar so the effects of shaft friction on the penetration of the T-bar could not be isolated. Nonetheless, the measured load was found to correlate well with the undrained shear strength of the clay at the tip of the T-bar.

The loads applied to the head of the pile and the T-bar were measured using miniature in-line compression-tension load cells from Futek having model-scale capacities of 1.1 kN, as shown in

Figure 5(a). The connection between the pile and the load cell incorporated a custom slip connection to the loading system so that the pile could have a free-head boundary condition during heating. Specifically, the slip connection allows the pile to be pushed downward into the soil layer during installation. After this, the loading system can be raised upward by a small increment until contact with the pile is lost, which permits the pile to be heated with no head restraint (i.e., the pile is free to expand upward during heating). After the heating and cooling cycle, the loading system is raised upward until the slip connection comes into contact with the internal bolt and initiates pile pullout. Horizontal brackets were connected to the top of the pile and T-bar to connect to digital linearly variable differential transformers (LVDTs) for monitoring displacements, as shown in Figure 5(a). The pore water pressure at different locations within the soil layer were measured using Druck PDCR81 miniature pore pressure transducers (PPTs) having a range of 0-1500 kPa. The sensors were inserted through ports in the side walls of the container after placement of the clay during the initial consolidation process that will be described below. To ease the sensor insertion to the targeted radial location in the soil layer, the sensor wire was strengthened by a thin steel rod connected to the transducer cable with heat shrink tubing as shown in Figure 5(b). A Swagelok Ultra-Torr fitting was used to provide a seal between the sensor cable and the container wall to prevent any leakage. Several thermocouples were used to measure the temperature in the soil at different depths and radial locations. The thermocouples were also strengthened with a thin steel rod in a similar manner to the PPTs as shown in Figure 5(c) so that they could be inserted into the clay horizontally through ports through the tank wall. In addition, K-type thermocouples were placed on the surface of the soil and on the outside of the container to measure the temperature of the boundaries. The soil surface deformation was monitored using an LVDT connected to a lightweight aluminum plate to provide a bearing platform.

Pictures of the data acquisition system components mounted on the centrifuge are shown in Figure 6. The temperature control unit for the heating element within the pile is shown in Figure 6(a), along with the computer used for temperature data acquisition. A National Instruments (NI) CompactDAQ chassis was used to acquire the temperature data, while an NI CompactRio chassis was used to acquire the force and displacement data and to control Haydon-Kerk stepper motors used to apply axial loads to the pile and T-bar, as shown in Figure 6(b).

MATERIALS

Kaolinite Clay

The soil used in the experiments was kaolinite clay obtained from M&M Clays Inc. of McIntyre, Georgia whose geotechnical properties are summarized in Table 2. The liquid limit of the kaolinite clay is 47, and the plastic limit was 28, so the clay classifies as CL according to the Unified Soil Classification Scheme (USCS). Results from an isotropic compression test indicates that the slopes of the normal compression line (λ) and the recompression line (κ) for the clay are 0.080 and 0.016, respectively. The hydraulic conductivity of the clay inferred from consolidation data ranges from 2.8×10^{-9} to 8.2×10^{-9} m/s for void ratios ranging from 1.05 to 1.45, respectively. The thermal pressurization response of this clay was characterized by Ghaaowd, the effects of temperature on the undrained shear strength of this clay were characterized by Samarakoon et al. (2018), and the thermal volume change of the clay was characterized by Samarakoon and McCartney (2020).

Ottawa Sand Bearing Layer

Ottawa F-65 sand was used as a drainage layer beneath the clay layer, and as a firm bearing layer for the energy pile upon insertion. The sand has a relatively uniform grain size distribution ranging from 0.1 to 0.5 mm. Its hydraulic conductivity varies from 0.0022 to 0.0012 m/s for the

loosest and densest states, respectively (Bastidas 2016), which is several orders of magnitude greater than that of the clay. The sand was tamped in moist conditions to reach a relative density of approximately 100% in both tests to form a stable bearing layer for the pile while still providing drainage for the clay layer.

MODEL CONSTRUCTION PROCEDURE

Approximately 45 kg of kaolinite clay in powder form was mixed with deaired water to form a slurry with a gravimetric water content of 135% within a vacuum mixer (a cement mixer with a sealed plate that permits application of vacuum to the mixing chamber). The clay slurry was then carefully poured into the container as shown in Figure 7(a). A layer of filter paper was placed at the top of the clay layer as shown in Figure 7(b). A porous stone having the same diameter as the inside of the container was lowered onto the surface of the slurry as shown in Figure 7(c) after which 24 hours were permitted for self-weight consolidation. The porous stone was manufactured of coarse sand mixed with 6% epoxy and reinforced with stainless steel mesh. A loading plate was then placed atop the porous stone as shown in Figure 7(d) and several dead weights were added in five 24-hour stages as shown in Figure 7(e), leading to a surcharge stress of 8 kPa. Changes in the vertical position of the steel loading plate were tracked using a micrometer, which were used to calculate changes in void ratio of the clay layer. A hydraulic piston connected to the top reaction plate was then used to apply higher axial stresses to the top of the clay layer as shown in Figure 7(e) until reaching a maximum surcharge stress of 21.7 kPa. A schematic of the clay layer with the hydraulic piston attached for 1 g consolidation is shown in Figure 8 (dead weights atop the steel weight are not shown). In some tests, a thermal needle connected to a KD2Pro thermal analyzer from Decagon Devices was included at the base of the clay layer at the location shown in Figure 8 to track the evolution in thermal conductivity with void ratio.

The compression curve of the clay layer measured during 1 g consolidation is shown in Figure 9(a). This curve is not from either of the two tests presented in this paper but is shown here as an example because the test corresponding to this curve was performed with a thermal needle. The vertical stresses correspond to those applied to the top of the clay layer with dead weights and the hydraulic piston and side friction may affect the vertical stress distribution within the specimen. The slope of the compression curve defined between the highest two vertical stresses was consistent with the compression index in Table 2. The void ratio achieved after this compression process varied slightly from test to test depending on the initial water content of the slurry, which was 130-135%. During the 1g compression process for the test in Figure 9(a), the variation in thermal conductivity with void ratio is shown in Figure 9(b). This figure also includes the results from thermal conductivity measurements made on kaolinite clay specimens in an isotropic triaxial test setup developed by McCartney et al. (2013) shown in Figure 2(b). A relatively linear trend between thermal conductivity and void ratio was obtained, and the results from two approaches follow a consistent trend despite the different stress states.

After 1 g consolidation of the clay layer, the applied load was removed and the top plate, porous stone, and filter paper were carefully removed. Approximately 60 mm of water was left above the clay layer to ensure the clay layer remained saturated. At the end of consolidation, the height of the clay layer ranged from 220-240 mm. The stepper motors for the pile and T-bar were connected to the top reaction plate, and the pile and T-bar were connected to the stepper motor loading rods. The top reaction plate was then slowly lowered into place on top of the container and fastened into place. Due the height limitation in the centrifuge basket above the top reaction plate, it was not possible to suspend the pile and T-bar completely outside of the clay layer at the beginning of the test. Accordingly, the pile had an initial penetration of approximately 124 mm in the clay layer,

and the T-bar was at an initial depth of 58 mm in the clay layer. It was still possible to install the pile to its final penetration depth at a constant displacement rate during centrifugation to simulate the jacked-in pile installation process, and the T-bar was able to characterize the undrained shear strength in the lower 2/3 of the clay layer. After this point, the thermocouples and pore water pressure sensors were inserted carefully through the ports in the container wall. After checking all sensors and performing safety checks, the centrifuge was then spun to 50 g.

TEST PROCEDURE

The centrifuge modeling methodology involved five testing stages, which are summarized in Table 3, and specific details of the tests performed according to his methodology will be discussed later. After a period of in-flight consolidation (Stage I), the pile was pushed to its final location at a constant displacement rate until the tip rested within the sand layer to result in end bearing conditions (Stage II), the pile was heated until reaching thermo-hydro-mechanical equilibrium as verified by the thermocouples and pore water pressure sensors embedded in the clay layer and in which case the pile is expected to expand upward due to the end bearing condition in sand (Stage III), was cooled until reaching thermo-hydraulic equilibrium and in which case the pile is expected to contract downward (Stage IV), then vertical pullout testing was performed (Stage V). An unheated pile was tested in the same manner as the heated pile except skipping Stages III and IV. The pile was pulled out at a constant model-scale displacement rate of 0.1 mm/s, which is fast enough in prototype scale to ensure undrained pullout conditions based on preliminary T-bar penetration tests with different rates. After this point, a push-pull T-bar test was performed after the unheated and heat pile tests. The T-bar test was performed at a model-scale radial distance of 75 mm from the pile (or $r_{T\text{-}bar}/r_{pile} = 6$), which was close enough to be affected by thermo-hydro-mechanical changes in the clay layer due to pile heating. The T-bar is close enough to be affected

by pile pullout, but sufficient time was permitted after pile pullout and performing the T-bar test to permit dissipation of excess pore water pressures (at least 5 hours). In the case of the unheated pile, Stages III and IV were skipped. After the centrifuge was spun down, the specimen was dissected to measure the gravimetric water content at different locations and to determine the final sensor locations. The final locations of the thermocouples and pore water pressure transducers in the heated pile test are shown in Table 4. A schematic of the assembled experimental setup showing the approximate locations of the sensors and the installed pile is shown in Figure 10(a), and a picture of the container on the basket is shown in Figure 10(b).

An example of the excess pore water pressure measured by a pore water pressure transducer (PPT4) during in-flight consolidation in one of the tests is plotted against the square root of time in Figure 11. This data permits definition of the value of t_{90} using the root time method (Taylor 1948) and permits evaluation of the end of primary consolidation. Due to the compression to normally consolidated conditions at 1 g followed by unloading then in-flight consolidation, the soil layer will be overconsolidated near the surface but normally consolidated below a model-scale depth of 60 mm (prototype-scale depth of 3 m) within the clay layer. Early tests reported by Ghaaowd et al. (2018) were performed with 7 PPTs, which were useful in confirming that the pore water pressure profile had reached hydrostatic conditions at the end of consolidation. Several of these PPTs were damaged in early tests, so the tests reported in this study only include two PPTs at the same radial location but different depths.

A picture of the pile and T-bar prior to installation is shown in Figure 12(a), while a picture of the installed pile and T-bar from the end of testing is shown in Figure 12(b). These figures demonstrate why a ponded water height of only 60 mm was used in testing to avoid submerging the load cells. The load penetration curves for the unheated and heated piles are shown in Figures

13(a) and 13(b), respectively. Although these curves were from two different clay layers, they have similar shapes. The piles were installed to the same penetration depth corresponding to the top of the sand layer, so the maximum axial force in both piles were slightly different and likely depend more on the sand layer than on the clay layer. The pile stepper motor rod was moved 3 mm upward to lose contact with the pile head, and the applied load was zeroed. After the pile was installed through the clay layer so that its tip was resting on the sand drainage layer, time was allowed for excess pore water pressures in the clay layer induced by pile installation to dissipate.

RESULTS

Time series of the main variables measured during testing on the unheated and heated piles are shown in Figure 14. As the goal of this study is not to scale the transient heat transfer and water flow processes, the time is shown in model scale. In the test on the unheated pile, the temperature of the pile was observed to be 20 °C and stable throughout the test, but this channel was unfortunately not recorded. The temperature at the surface of the clay layer shown in Figure 14(a) indicated that the surface was slightly cooler and was approximately 18 °C at the time of pile installation. In the test on the heated pile, the entire soil layer and pile were approximately 21 °C until the pile was heated to a target temperature 65 °C. The elevated temperature was maintained for approximately 30 hours, which was sufficient to reach thermo-hydraulic equilibrium in the clay surrounding the energy pile (i.e., stable temperature and pore water pressures). This was followed by ambient cooling for 6 hours, which was observed to be sufficient for the clay temperature and pore water pressure to stabilize. During heating, it took approximately 5 hours to reach the target temperature, and the temperatures in the soil at different radial locations were lower and took longer to stabilize.

The pore water pressure time histories during the unheated pile test are shown in Figure 14(c). After reaching the end of primary consolidation, the pore water pressures increased sharply during pile installation in Stage II, which stabilized after approximately 10 hours. The pore water pressures also increased sharply during pile pullout in Stage V. The pore water pressures sensors in the heated pile tests were at different locations than in the unheated pile test, so the initial pore water pressures measured by PPT3 and PPT4 were different. Nonetheless, similar behavior was noted in the heated pile test in Figure 14(d) until the time of pile heating. At this point a smaller increase in pore water pressure was observed than the magnitude of pore water pressure changes during pile installation. During pile cooling, a decrease in pore water pressure below hydrostatic conditions was observed. This negative pore water pressure may reflect that cooling was faster than the rate of drainage. The pore water pressures stabilized before pullout, which also led to a large increase in pore water pressure.

The pile head displacement in the unheated test is shown in Figure 14(e). Unfortunately, the long stroke of the LVDT necessary to track the installation and pullout of the pile meant that the small changes in pile head movement during heating were close to the resolution of the LVDT. Nonetheless, a decrease in pile head position was observed after pile installation, which may be due to time dependent dragdown on the pile. The pile head displacement in the heated pile test shown in Figure 14(f) is interesting as it was expected that the pile would expand upward during heating. However, less downward movement was observed in the heated pile than in the unheated pile, which may imply that the upward movement of the pile due to thermal expansion was compensating against the downward movement arising from time-dependent downdrag. During the cooling stage, the pile head moved downward by approximately 0.28 mm due to the pile thermal contraction. This downward movement corresponds to an axial strain of 1080 με for the

decrease in temperature of 45 °C. The linear coefficient of thermal expansion for the pile is approximately 24 με/°C, which is consistent with the linear coefficient of thermal expansion of aluminum of 23 με/°C.

There was not a thermocouple at the same location as PPT3 and PPT4, so the time series of temperature at a model-scale radius of 62 mm was linearly interpolated from the measurements of TC3 and T4, as shown in Figure 15(a). For a change in temperature of approximately 13 °C an increase in pore water pressure of approximately 4 kPa was observed at both depths. This is lower than the change in pore water pressure expected for fully undrained conditions of 15.8 kPa at the depth of PPT4 and 16.9 kPa at the depth of PPT3 predicted using the model of Ghaaowd et al. (2017) for the effective stress and void ratio at the depth of these PPTs. The lower maximum pore water pressures measured at these depths is attributed to partial drainage, as drainage will start to occur as soon as pore water pressures are generated. Further, based on the model of Ghaaowd et al. (2017) it was expected that the deeper PPT would have recorded a higher change in pore water pressure associated with a higher effective stress and consolidation to a lower void ratio. This inconsistent trend between the measurements of PPT3 with the predicted trend with depth from the model of Ghaaowd et al. (2017) is mainly attributed to partial drainage as PPT3 was closer to the sand drainage layer, although it possible that the actual temperature at the location of PPT4 is higher than at the location of PPT3 (and different from the temperature at the same radial location as the two PPTs obtained by the linear interpolation between the measurements of TC3 and TC4).

The radial distribution in temperature at model scale after different times is shown in Figure 16. Although the pile temperature reached 65 °C, which corresponded to an increase in temperature of 45 °C, the soil temperature only increased by at most 22 °C for the locations monitored. It is expected that larger changes in temperature, which correspond to greater changes in pore water

pressure and thermal consolidation, may have occurred close to the pile surface. Nonetheless, after 30 hours of heating the pile had a zone of influence of approximately 150 mm. The outer boundary at a radial distance of 275 mm did not appear to influence the radial distribution in temperature.

The load-displacement curves for the heated and unheated piles during pullout are shown in Figure 17, where a negative force is used to denote the tensile force measured by the load cell. The maximum temperatures are shown in the legend of this figure to differentiate the unheated and heated piles, but both pullout tests were performed at a room temperature of approximately 20 °C. The force and pile displacement were zeroed at the point where the pile first started to move upward. The pullout capacities for the unheated and heated piles are -1004 and -1434 kN respectively, occurring at displacements of 0.09 and 0.16 m in prototype scale, respectively. The pullout capacity of the heated pile was 1.43 times greater than that of the unheated pile. It should be noted that the pile self-weight is 542 kN, so the self-weight makes up approximately half of the pullout capacity of the unheated pile. It was interesting that the slope of the load-displacement curve for the heated pile is only slightly greater than that of the unheated pile. This may be because of the large coefficient of thermal expansion of the aluminum pile, which led to the mobilization of side shear stresses before pullout occurred in the heated pile test. Although the pile likely contracted after cooling, the heating-cooling cycle may have led to a softening response in the load-displacement curve even though an increase in pullout capacity with increased temperature is still observed. After reaching the pullout capacity, both piles show a softening response for the displacement range shown. However, the heated pile shows a greater amount of softening. Similar increases in pullout capacity were observed by Ghaaowd and McCartney (2018a, 2018b) for energy piles with a fixed head boundary condition during heating.

The T-bar measurements in the clay layers with heated and not heated energy piles may help understand the effects of heating and cooling on the behavior of normally consolidated clay layers. To infer the profile of undrained shear strength in the clay layer, the T-bar was inserted into clay layer at speed of 0.2 mm/s until reaching a maximum depth of 220 mm, which was close to the bottom of the clay layer. As mentioned, due to the stroke limitation of the T-bar motor and the space restriction within the centrifuge container, the initial position of the T-bar was at an initial depth corresponding to 1/3 of the clay layer thickness. After reaching the maximum stroke, the T-bar was extracted at the same speed from the clay layer until returning to its initial position. The undrained shear strength was interpreted from the correlations of Stewart and Randolph (1991):

$$c_u = \frac{F_v}{N_b D L} \quad (1)$$

where c_u is the undrained shear strength, D is the T-bar diameter of 14 mm, L is the T-bar length of 57 mm, F_v is the measured T-bar force (positive for insertion and negative for extraction), and N_b is the T-bar bearing factor. The T-bar bearing factor was calculated using the equation proposed by Oliveira et al. (2010):

$$N_b = 0.0053\left(\frac{H}{D}\right)^6 - 0.1102\left(\frac{H}{D}\right)^5 + 0.9079\left(\frac{H}{D}\right)^4 - 3.7002\left(\frac{H}{D}\right)^3 + 7.2509\left(\frac{H}{D}\right)^2 - 3.9168\left(\frac{H}{D}\right) + 5.3519 \quad (2)$$

where H is the height of soil above the T-bar. In their model the value of the T-bar bearing factor N_b should be in the range of 5.14 to 10.50.

The profile of undrained shear strength from the T-bar test next to the unheated pile is shown in Figure 18. The "positive" undrained shear strength values are for insertion into the intact lower 2/3 of the clay layer and the "negative" undrained shear strength values are for extraction from the disturbed clay layer. The undrained shear strength is always positive, but it is conventional to show

hysteresis loops like those in Figure 18 for analysis of T-bar tests (Oliveira et al. 2010). To check the undrained shear strengths from the T-bar tests, the undrained shear strengths were also interpreted from the force-displacement data from pile insertion presented in Figure 13. Specifically, the equations for side shear capacity Q_s and end bearing capacity Q_p of a pile in an undrained clay layer were used to back-calculate the undrained shear strength at a given depth of penetration $H_{penetration}$:

$$Q = Q_s + Q_p \quad (3)$$

$$Q_s = \alpha\, c_u\, A_s = c_u\, \pi\, D\, H_{penetration} \quad (4)$$

$$Q_p = 9\, c_u\, A_p = 2.25\, \pi\, D^2\, c_u \quad (5)$$

where α is the side shear factor (assumed to equal 1.0 for soft clays), A_s is the pile surface area, and A_p is the point bearing area of the pile. Specifically, the undrained shear strength can be estimated from the pile penetration as follows:

$$c_u = Q / (\pi\, D\, H_{penetration} + 2.25\, \pi\, D^2) \quad (6)$$

The interpreted undrained shear strength profiles interpreted from pile penetration data are also shown in Figure 18(a). A good match is observed with the undrained shear strength profile from the T-bar in the lower portion of the clay layer. The average measured undrained shear strength by using the T-bar was 10 kPa (close to the value of 11 kPa obtained from pile insertion in Figure 18(a)) and Equation 3 was used to estimate the pullout capacity of 431 kN. When the pile weight of 542 kN is added to this, the total pullout force is 973 kN, which is close to the measured pullout capacity from the unheated pile test.

A comparison of the T-bar test results from the tests on the unheated and heated piles is shown in Figure 18(b). Although the T-bar is located at a model-scale distance of approximately 100 mm from the pile where the change in temperature was only about 8 °C, a slightly greater undrained

shear strength profile was observed during insertion. During extraction, the same undrained shear strength was observed. The greatest change in undrained shear strength is expected at the soil-pile interface, but the T-bar results in this figure indicate that improvement may occur in the surrounding soil as well. Specifically, the spatial distribution of thermally induced changes in pore water pressure and thermal consolidation will follow the change in temperature in the soil and the excess pore water pressures will dissipate radially away from the energy pile.

After the pile pullout and T-bar tests, the centrifuge was spun down and the container was removed. The final height of the clay layer was measured, and samples of clay were taken at different locations within the clay layer. Also, the final locations of the sensors around the pile were measured, with the final sensor locations for the heated pile test summarized in Table 4. The post-test measurements of the gravimetric water content are shown in Figures 19(a) and 19(b) for the tests on the unheated and heated piles, respectively. The initial void ratios achieved after 1g consolidation in each of the tests are shown in these figures, with the unheated pile test having a slightly lower initial void ratio of 1.35 than the heated pile test which had an initial void ratio of 1.45. In both clay layers, lower void ratios were observed near the center of the clay layer, and a clear swelling is observed near the clay surface, reflected in the some of the final void ratios near the clay surface being greater than the initial void ratios. The lower void ratios near the center of the clay layer in both tests may have been due to the densification associated with dissipation of excess pore water pressures generated by pile installation. Although the depths of the samples in each test make it difficult to visualize trends, the changes in void ratio near the center of the clay layer were greater for the heated pile test, ranging from 0.1 near the clay surface to 0.45 near the pile toe. The changes in void ratio near the center of the clay layer for the unheated pile test ranged from 0.1 near the clay surface to 0.36 near the pile toe. It is possible that the difference in the

change in void ratios of the clay layers in the heated and unheated pile tests could be partly attributed to the rapid rate of cooling in the heated pile test, which may result in some partial recovery of thermal contractions as observed by Samarakoon and McCartney (2020) in thermal triaxial tests on this clay. It is possible that lower void ratios may have been measured at the pile interface in the heated pile test, but unfortunately this data was not collected. The greater change in void ratios near the center of the clay layer in the heated pile test support the improvement due to thermal consolidation with the pullout results in Figure 17 and the T-bar tests in Figure 18. In addition, similar observations in pullout results and T-bar tests were made in other tests on heated pile restrained head conditions reported by Ghaaowd and McCartney (2018) and Ghaaowd et al. (2018).

CONCLUSION

This paper described the development of a new centrifuge modeling methodology that can be used to understand the impacts of using an energy pile to improve the mechanical properties of saturated clays, leading to an increase in pullout capacity. Time series of temperature, pore water pressure, and deformation were interpreted to understand the transient process of soil improvement. Despite small changes in pore water pressure during heating and small changes in void ratio at the end of testing, the pullout capacity of pile heated from 20 to 65 °C before being cooled to 20 °C was significantly greater than the pullout capacity of a pile at 20 °C. Interpretation of the unheated pile pullout capacity using undrained shear strengths from T-bar tests shows good agreement with measured values. Undrained shear strength values after the heating-cooling cycle from T-bar tests showed improvement even at distances away from the pile.

Overall, the centrifuge testing methodology provides useful insight into the transient thermal consolidation process under realistic boundary conditions and stress states and provides useful data

for validation of numerical simulations. The main implication of the typical results from the testing methodology presented in this study is that heating can be used to improve the undrained shear strength of normally consolidated soil surrounding offshore foundations. This provides a practical advantage as the pile can be installed into the ground with ease, then improved using heat generated within the pile without the need to apply mechanical stresses to the clay layer. The testing approach presented in this study can help provide guidance on the appropriate temperature range to apply to energy piles to reach a desired level of improvement in pullout capacity and can help provide guidance on the time required to apply a temperature boundary condition in the field.

REFERENCES

Abuel-Naga, H.M., Bergado, D.T., and Chaiprakaikeow, S. (2006). "Innovative thermal technique for enhancing the performance of prefabricated vertical drain during the preloading process." Geotextiles and Geomembranes, 24, 359–370.

Abuel-Naga, H.M., Bergado, D.T., Bouazza, A. (2007a). "Thermally induced volume change and excess pore water pressure of soft Bangkok clay." Engineering Geology. 89, 144-154.

Abuel-Naga, H. M., Bergado, D. T., Bouazza, A. and Ramana, G.V. (2007b). "Volume change behavior of saturated clays under drained heating conditions: experimental results and constitutive modeling." Canadian Geotechnical Journal. 44(8), 942-956.

Artidteang, S., Bergado, D.T., Saowapakpiboon, J., Teerachaikulpanich, N. and Kumar, A. (2011). Enhancement of efficiency of prefabricated vertical drains using surcharge, vacuum and heat preloading, Geosynthetics International, 18(1), 35–47.

Baldi, G., Hueckel, T., Pellegrini, R. (1988). "Thermal volume changes of the mineral-water system in low-porosity clay soils." Canadian Geotechnical Journal. 25(4), 807-825.

Bastidas, A.M. (2016). Ottawa F-65 Sand Characterization. Ph.D. Dissertation, University of California, Davis.

Bergenstahl, L., Gabrielsson, A., Mulabdic, M., (1994). "Changes in soft clay caused by increases in temperature." Proc. 13th Int. Conf. on Soil Mech. and Found. Eng., New Delhi, pp. 1637–1641.

Brandl, H. (2006). "Energy foundations and other thermo-active ground structures." Géotechnique. 56(2), 81-122.

Booker, J.R. and Savvidou, C. (1985). "Consolidation around a point heat source." International Journal for Numerical and Analytical Methods in Geomechanics. (9), 173-184.

Burghignoli, A., Desideri, A., and Miliziano, S. (2000). "A laboratory study on the thermomechanical behavior of clayey soils." Canadian Geotechnical Journal. 37(4), 764-780.

Campanella, R.G., and Mitchell, J.K. (1968). "Influence of temperature variations on soil behavior." Journal of the Soil Mechanics and Foundation Division, 94(SM3), 709-734.

Chen, D. and McCartney, J.S. (2017). "Parameters for load transfer analysis of energy piles in uniform nonplastic soils." ASCE International Journal of Geomechanics. 17(7), 04016159.

Ghaaowd, I., Takai, A., Katsumi, T. and McCartney, J.S. (2017). "Pore water pressure prediction for undrained heating of soils." Environmental Geotechnics. 4(2): 70-78.

Ghaaowd, I., McCartney, J.S., Huang, X., Saboya, F., and Tibana, S. (2018a). "Issues with centrifuge modeling of energy piles in soft clays." Proceedings of the 9th International Conference on Physical Modeling in Geotechnics: Physical Modelling in Geotechnics. A. McNamara et al., eds. Taylor & Francis Group, London. 1365-1370.

Ghaaowd, I. and McCartney, J.S. (2018b). "Centrifuge modeling of temperature effects on the pullout capacity of energy piles in clay." DFI 43rd Annual Conference on Deep Foundations. Anaheim, CA. Oct 24-27. 1-7.

Houston, S.L., Houston, W.N., and Williams, N.D. (1985). "Thermo-mechanical behavior of seafloor sediments." Journal of Geotechnical Engineering. 111(12), 1249-1263.

Hueckel, T., Pellegrini, R. and Del Omo, C. (1998). "A constitutive study of thermo-elastoplasticity of deep carbonatic clays," International Journal of Numerical and Analytical Methods in Geomechanics, Vol. 22, No. 7, pp.549-574.

Knellwolf, C., Peron, H., and Laloui, L. (2011). "Geotechnical analysis of heat exchanger piles." J. Geotech. Geoenviron. Eng., 10.1061/(ASCE)GT.1943-5606.0000513, 890–902.

Kutter, B. (1992). "Dynamic centrifuge modeling of geotechnical structures." Transportation Research Record. 1336, 24-30.

Laloui, L., Nuth, M., and Vulliet, L. (2006). "Experimental and numerical investigations of the behaviour of a heat exchanger pile." International Journal of Numerical and Analytical Methods in Geomechanics. 30, 763-781.

Cekerevac, C., Laloui, L., and Vuilliet, L. (2005). "A novel triaxial apparatus for thermo-mechanical testing of soils." Geotechnical Testing Journal. 28(2), 1-10.

Laloui, L., Nuth, M., and Vulliet, L. (2006). "Experimental and numerical investigations of the behavior of a heat exchanger pile." International Journal of Numerical and Analytical Methods in Geomechanics. 30, 763-781.

Maddocks, D.V. and Savvidou, C. (1984). "The effect of the heat transfer from a hot penetrator installed in the ocean bed." Proc. Symp. on the Application of Centrifuge Modeling to Geotechnical Design. W.H. Craig. Manchester U.K

McCartney, J.S. and Murphy, K.D. (2017). "Investigation of potential dragdown/uplift effects on energy piles." Geomechanics for Energy and the Environment. 10(June), 21-28.

Murphy, K.D. and McCartney, J.S. (2015). "Seasonal response of energy foundations during building operation." Geotechnical and Geological Engineering. 33(2), 343-356.

Murphy, K.D., McCartney, J.S., and Henry, K.S. (2015). "Evaluation of thermo-mechanical and thermal behavior of full-scale energy foundations." Acta Geotechnica. 10(2), 179 195.

Ng, C.W.W., Gunawan, A. and Laloui, L. (2014). "Centrifuge modelling of energy piles subjected to heating and cooling cycles in clay." Géotechnique Letters, 4(4), 310-316.

Ng, C.W.W., Zhang, C., Farivar, A., and Gomaa, S.M.M.H. (2019). Scaling effects on the centrifuge modelling of energy piles in saturated sand. Géotechnique Letters 10(1), 57-62.

Nicholson, P.G. (2015). Soil Improvement and Ground Modification Methods. Butterworth-Henemann. Oxford.

Oliveira, J.R.M.S., Almeida, M.S.S. Almeida, M.C.F. and Borges, R.G. (2010). "Physical modeling of lateral clay-pipe interaction." Journal of Geotechnical and Geoenvironmental Engineering. 136(7), 950–956.

Pothiraksanon, C., Bergado, D.T. and Abuel-Naga, H.M. (2010). "Full-scale embankment consolidation test using prefabricated vertical thermal drains." Soils and Foundations, 50(5): 599-608.

Salager, S., Laloui, L. and Nuth, M. (2012). "Efficiency of thermal vertical drains for the consolidation of soils." 2nd Int. Conf. on Transportation Geotechnics, Hokaido, Japan. 1-10.

Samarakoon, R., Ghaaowd, I. and McCartney, J.S. (2018). "Impact of drained heating and cooling on undrained shear strength of normally consolidated clay." Energy Geotechnics: SEG-2018.

Proceedings of the 2nd International Symposium on Energy Geotechnics. Lausanne, Switzerland. Sep. 26-28. A. Ferrari, L. Laloui, eds. Springer, Vienna. 243-249.

Samarakoon, R., and McCartney, J.S. (2020). "Role of initial effective stress on the thermal consolidation of normally consolidated clays." Proc. 2nd International Conference on Energy Geotechnics (ICEGT-2020). La Jolla, CA. Mar. 28-31, 2021. E3S Web of Conferences, Les Ulis, France. pp. 1-6.

Savvidou, C. (1988). "Centrifuge modelling of heat transfer in soil." Proc. Centrifuge 88. Balkema. 583–591.

Stewart, D. and Randolph, M. (1994). "T-Bar penetration testing in soft clay." Journal of the Geotechnical Engineering Division. ASCE. 120(12): 2230-2235.

Stewart, M.A. and McCartney, J.S. (2014). "Centrifuge modeling of soil-structure interaction in energy foundations." ASCE Journal of Geotechnical and Geoenvironmental Engineering. 140(4), 04013044-1-11.

Sultan, N., Delage, P., and Cui, Y.J. (2002). "Temperature effects on the volume change behavior of boom clay." Engineering Geology. 64, 135-145.

Takai. A., Ghaaowd, I., Katsumi, T., McCartney, J.S. (2016). "Impact of drainage conditions on the thermal volume change of soft clay." GeoChicago 2016: Sustainability, Energy and the Geoenvironment. Chicago. Aug. 14-18. pp. 32-41.

Towhata, I., Kuntiwattanakul, P., Seko, I., and Ohishi, K. (1993). "Volume change of clays induced by heating as observed in consolidation tests." Soils and Foundations. 33(4), 170-183.

Taylor, D.W. 1948. Fundamentals of Soil Mechanics. John Wiley and Sons, New York.

Uchaipichat, A. Khalili, N. "Experimental investigation of thermo-hydro-mechanical behaviour of an unsaturated silt." Géotechnique. 59(4), (2009), 339–353.

Vega, A. and McCartney, J.S. (2015). "Cyclic heating effects on thermal volume change of silt." Environmental Geotechnics. 2(5), 257-268.

Yazdani S., Helwany S., and Olgun G. 2019. "Investigation of thermal loading effects on shaft resistance of energy pile using laboratory-scale model." Journal of Geotechnical and Geoenvironmental Engineering, 145(9): 04019043.

Yazdani S., Helwany S., and Olgun G. (2020). "The mechanisms underlying long-term shaft resistance enhancement of energy piles in clays." Canadian Geotechnical Journal. https://doi.org/10.1139/cgj-2019-0236.

Zeinali, S.M. and Abdelaziz, S.L. (2021). "Thermal consolidation theory." Journal of Geotechnical and Geoenvironmental Engineering. 147(1), 04020147.

TABLE 1. Details of the UCSD Actidyne C61-3 geotechnical centrifuge

Quantity	Value
Rated capacity (g-tons)	50
Radius to basket (m)	2.0
Basket width (m)	0.6
Basket length (m)	1.0
Basket depth (m)	0.6
Maximum centripetal acceleration (g)	130
Maximum capacity under maximum acceleration (kg)	230
Maximum capacity (kg)	500
Maximum acceleration under maximum capacity (g)	100

TABLE 2. Properties of the kaolinite clay used in this study.

Property	Value
Liquid limit	47
Plastic limit	28
Plasticity index	19
Specific gravity	2.6
C_c	0.230
C_r	0.037

TABLE 3. Summary of testing stages

Testing Stage	Stage Description
I	In-flight consolidation
II	Pile installation
III	Pile heating
IV	Pile cooling
V	Pile pullout

TABLE 4. Sensor locations in heated pile test determined after testing

Sensor	r (mm)	z (mm)
TC1	36	142
TC2	94	162
TC3	46	102
TC4	81	112
TC5	101	122
TC6	146	122
PPT3	62	150
PPT4	62	140

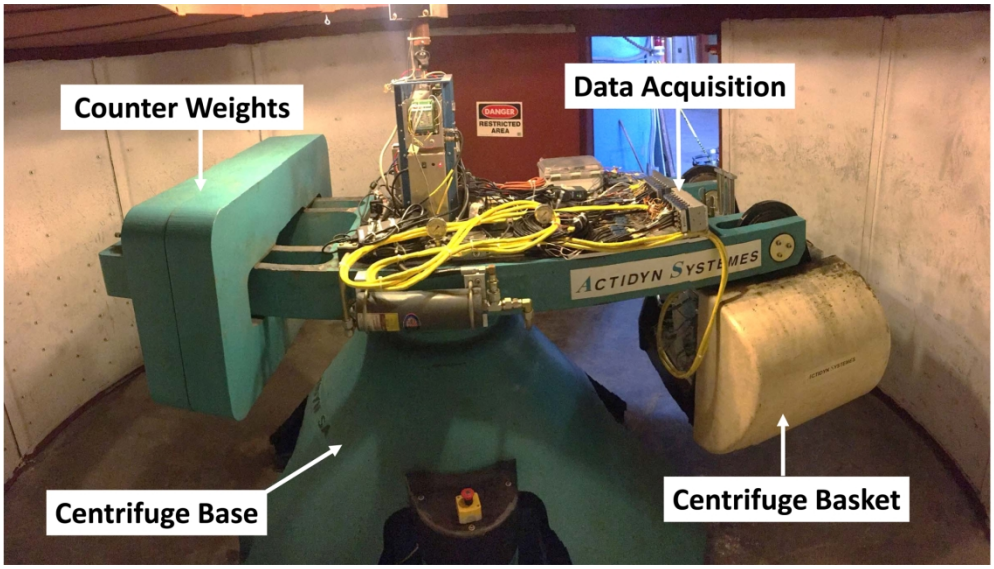

FIG. 1. UCSD geotechnical centrifuge.

88x49mm (600 x 600 DPI)

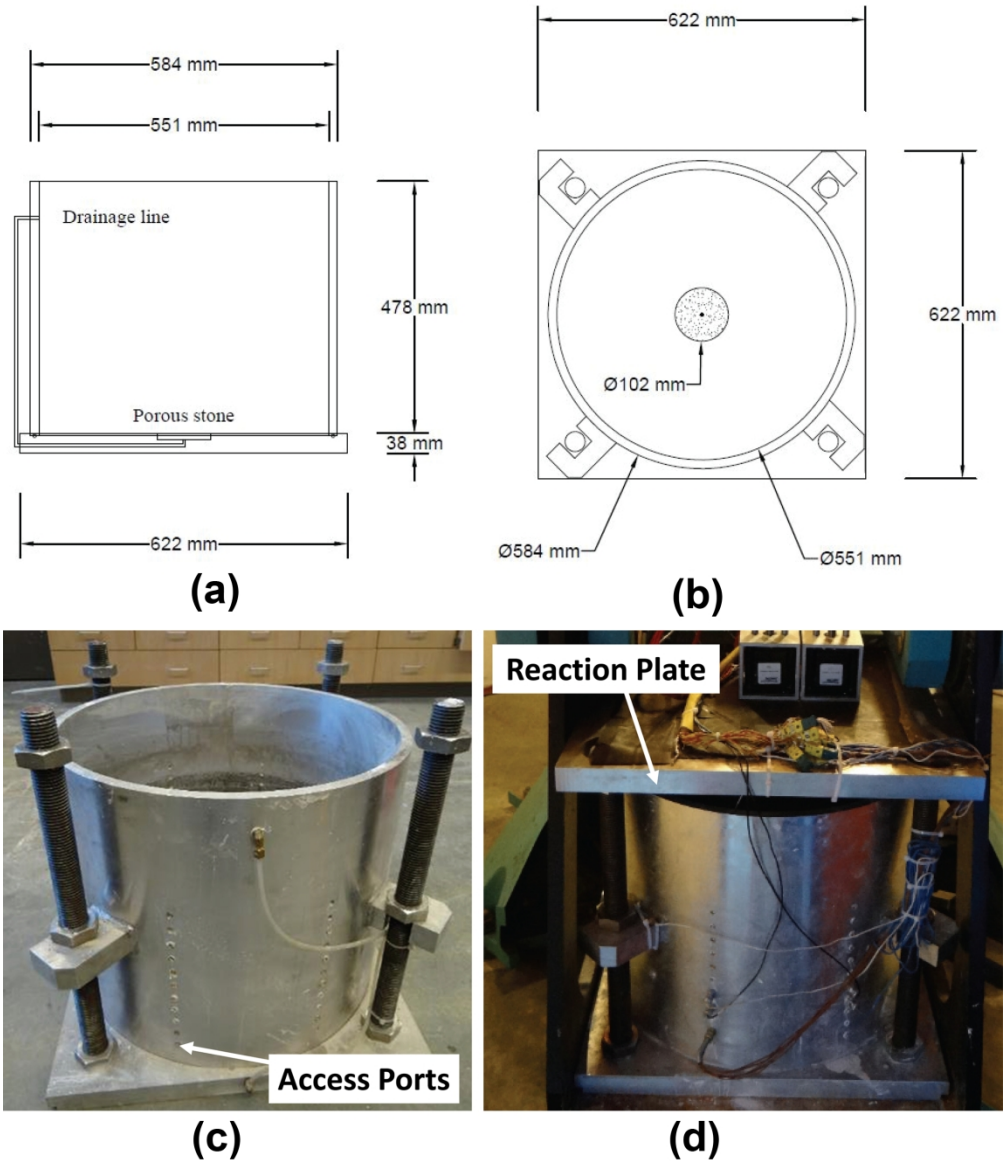

FIG. 2. Cylindrical centrifuge container with reaction plate for load application: (a) Cross section schematic, (b) Plan view schematic, (c) Container without reaction plate showing access ports at different heights from base; (d) Container with reaction plate inside the centrifuge.

101x120mm (600 x 600 DPI)

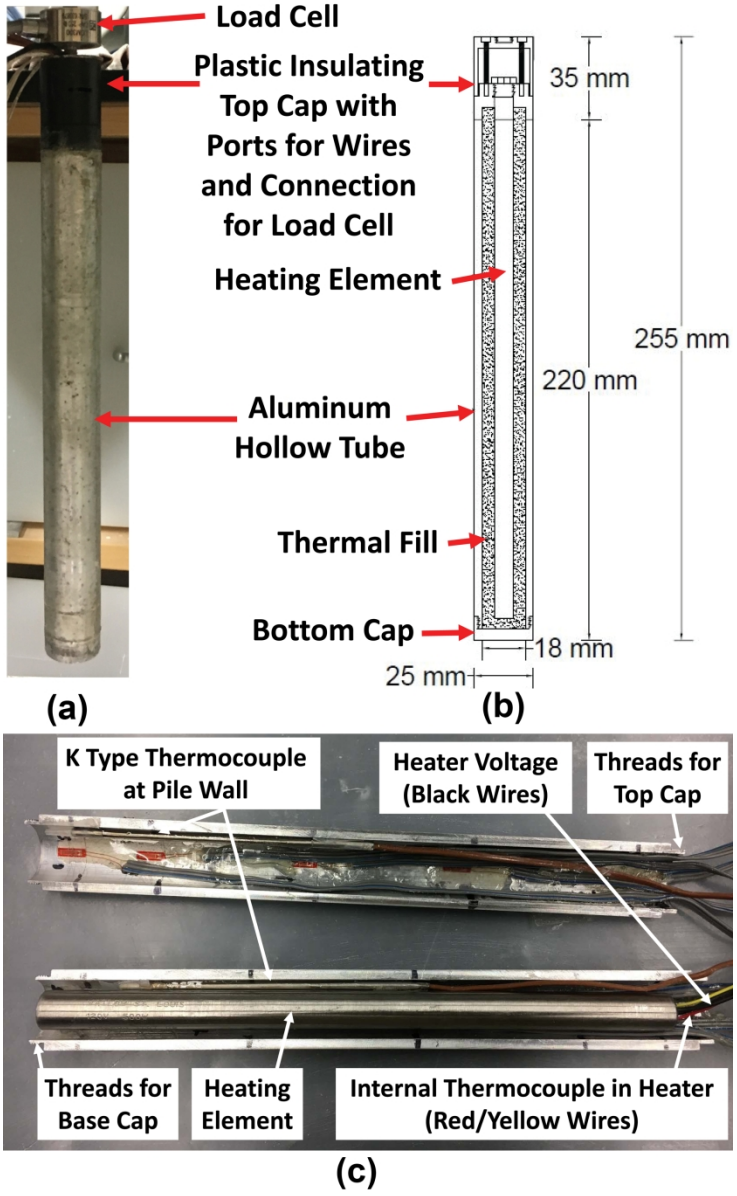

FIG. 3. Details of the centrifuge-scale energy pile with internal heating element: (a) Assembled pile, (b) Pile cross section with model-scale dimensions, (c) Disassembled pile showing heating rod and internal instrumentation.

88x145mm (600 x 600 DPI)

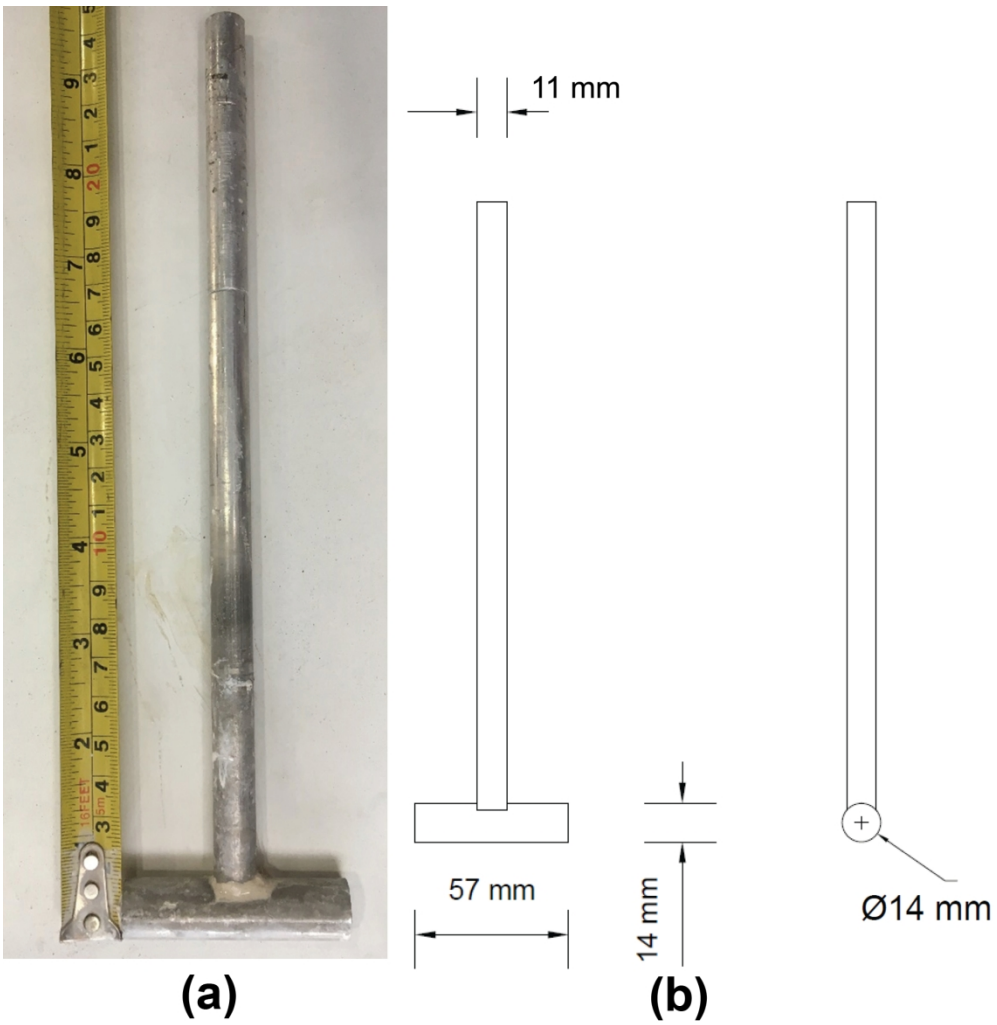

FIG. 4. T-bar for soil characterization before and after pile heating: (a) Photo; (b) Schematics.

88x90mm (600 x 600 DPI)

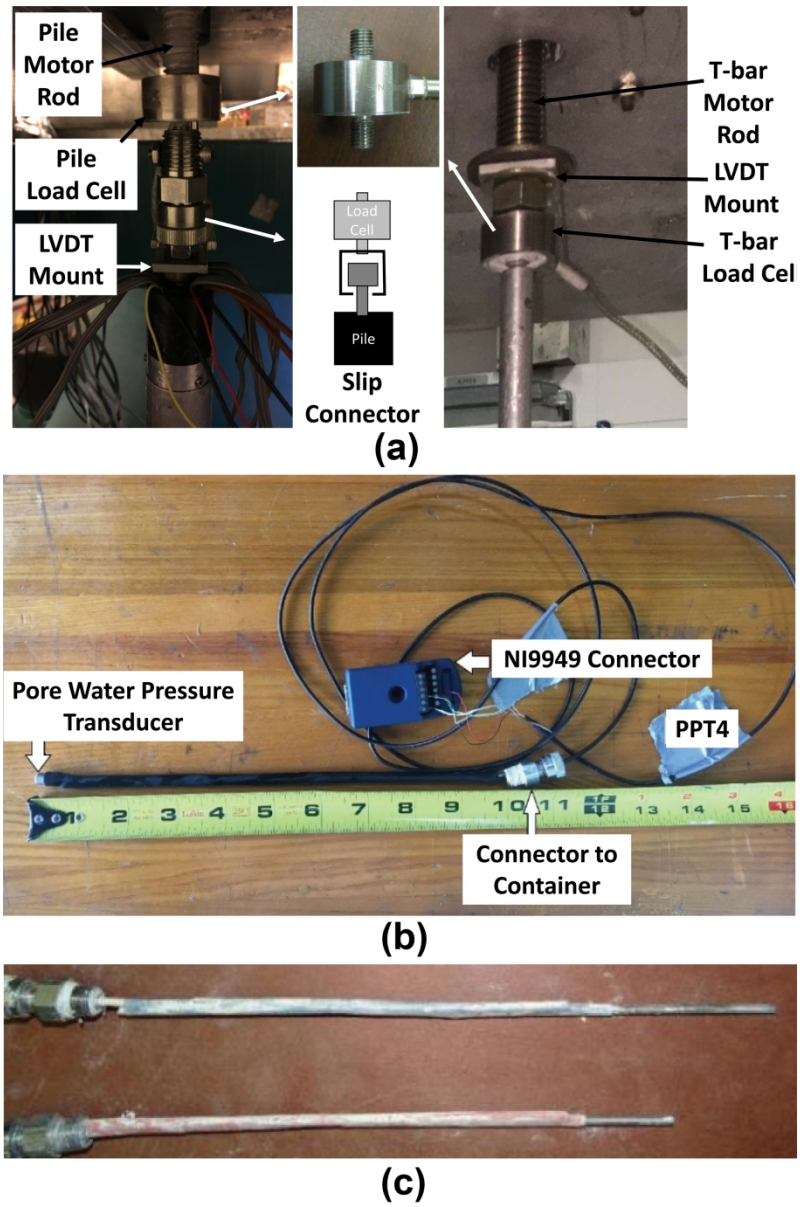

FIG. 5. Key instrumentation: (a) Miniature inline threaded load cells attached to the pile head and T-bar; (b) Miniature Druck pore water pressure transducers connected to a rigid rod for horizontal insertion; (c) K-type thermocouples having different lengths connected to rigid rods for horizontal insertion.

88x134mm (600 x 600 DPI)

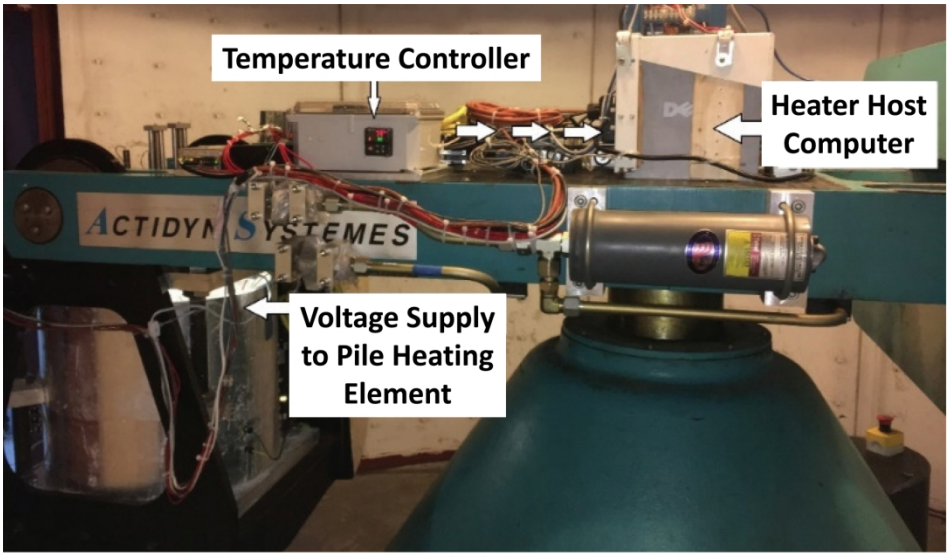

(a)

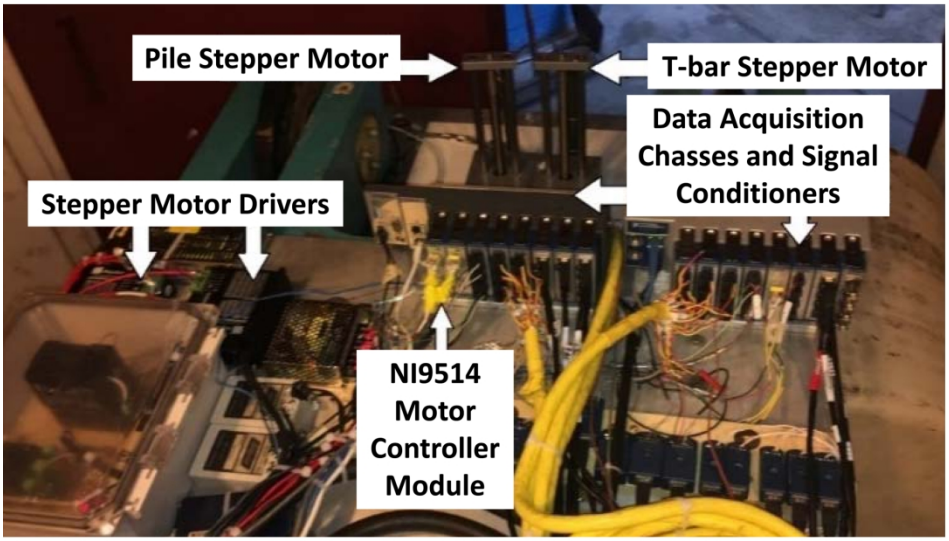

(b)

FIG. 6. Centrifuge data acquisition system components: (a) Pile heat controller components; (b) Data acquisition chasses with signal conditioning units and motor controller modules along with motor control hardware.

88x112mm (600 x 600 DPI)

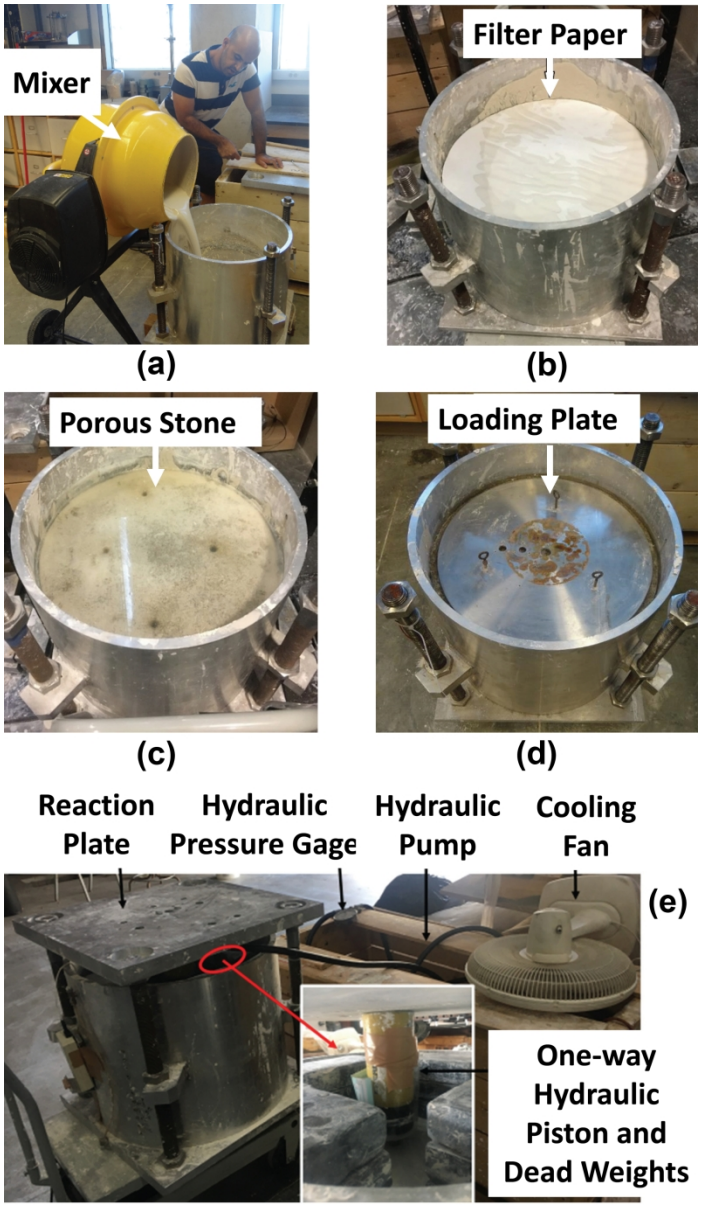

FIG. 7. Soil preparation procedures: (a) Placing the mixed slurry in the container; (b) Filter paper placement; (b) Filter paper placement on the top of clay layer; (c) Porous stone on top of clay slurry mix; (d) Placement of loading plate on top of porous stone; (e) Slurry pre-consolidated under dead weights at 1 g.

88x153mm (600 x 600 DPI)

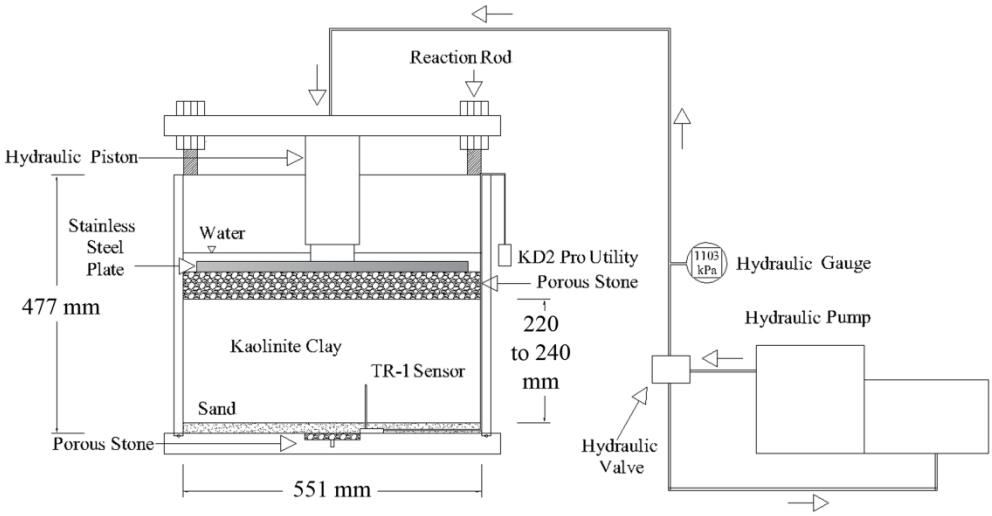

FIG. 8. Schematic of the container with the reaction plate during 1-g consolidation showing the thermal needle (TR-1 Sensor).

178x90mm (599 x 599 DPI)

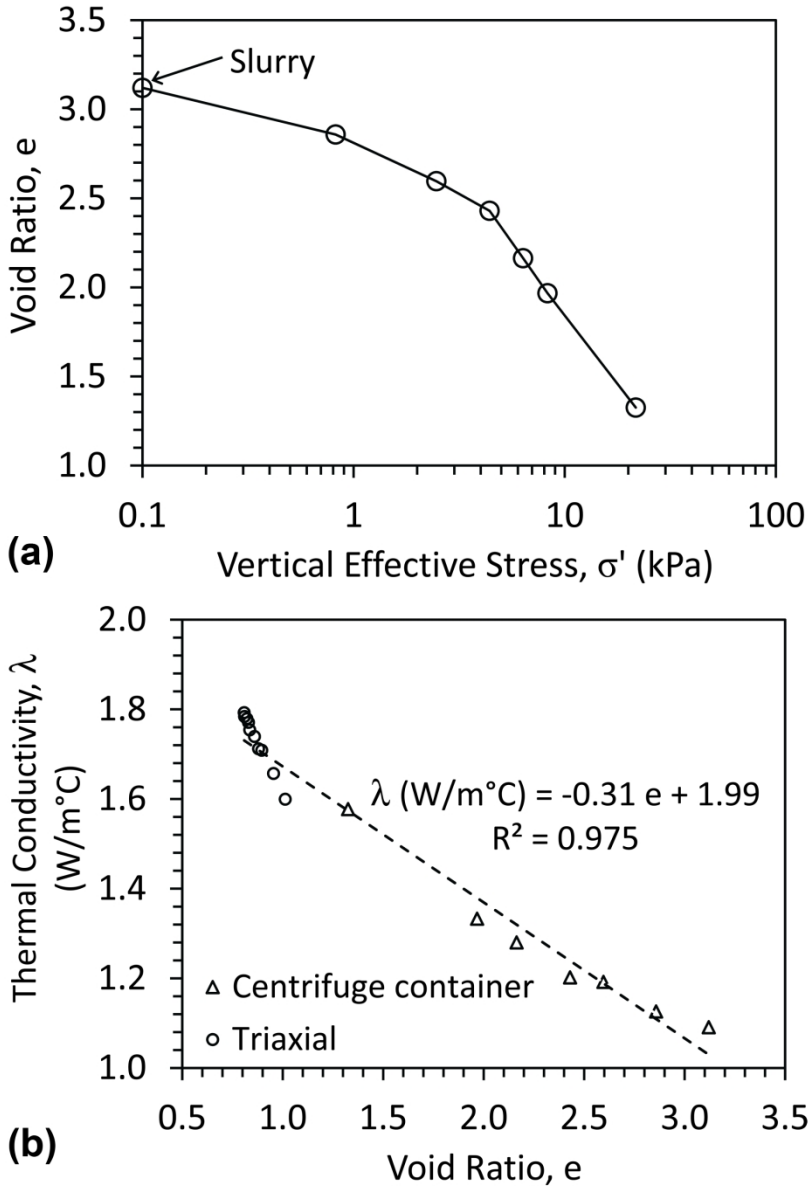

FIG. 9. Typical data obtained from 1 g consolidation of the clay layer: (a) Compression curve; (b) Thermal conductivity as a function of void ratio for the clay along with a comparison from thermal needle tests on isotropically consolidated clay specimens in a triaxial cell.

88x128mm (600 x 600 DPI)

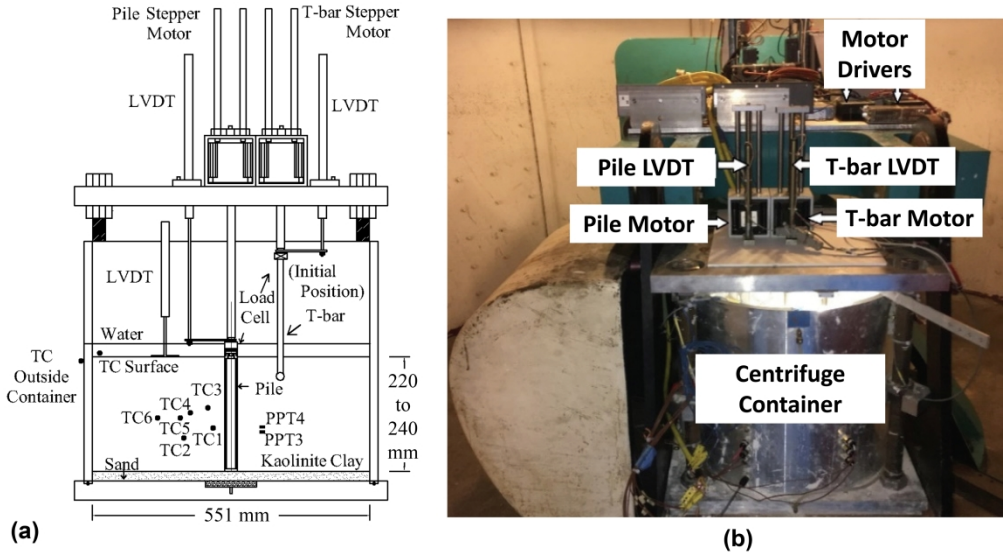

FIG. 10. System configuration for testing of energy piles in soft clay: (a) Cross-section schematic with approximate locations of sensors; (b) Picture of stepper motors mounted to the reaction plate prior to testing.

177x98mm (600 x 600 DPI)

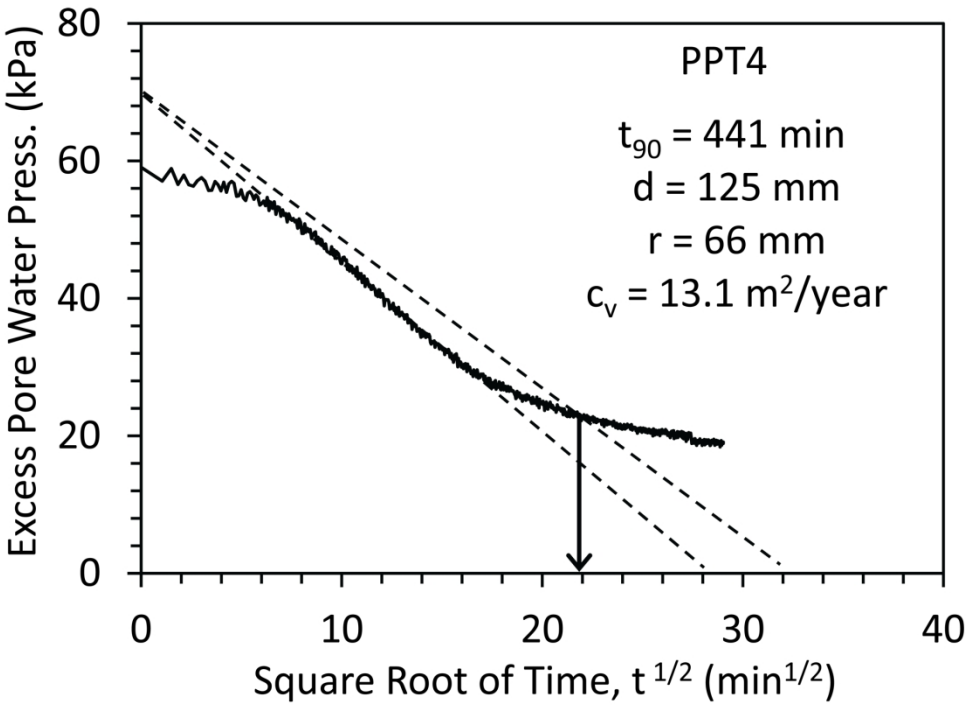

FIG. 11. Example of in-flight consolidation results in the centrifuge

88x63mm (600 x 600 DPI)

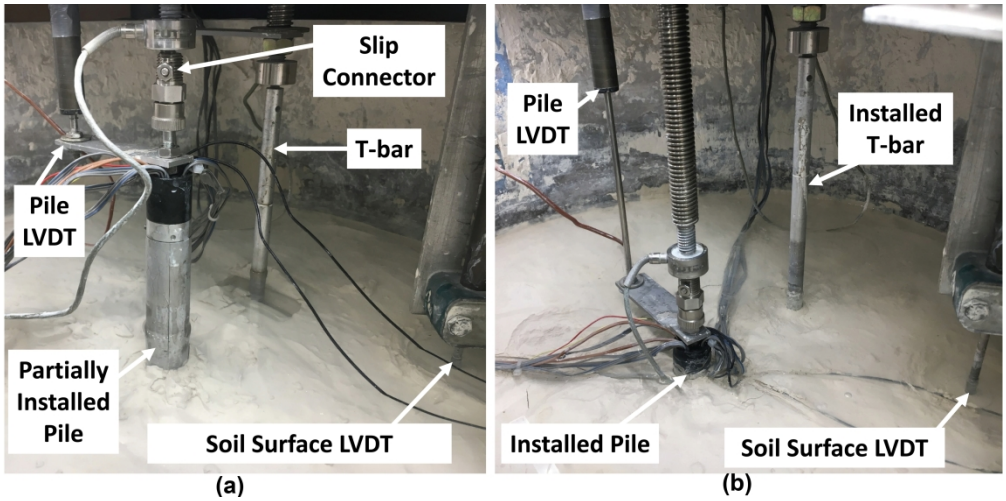

FIG. 12. In-flight pictures of the energy pile and T-bar: (a) At the initial partially-installed positions; (b) After installation.

177x87mm (600 x 600 DPI)

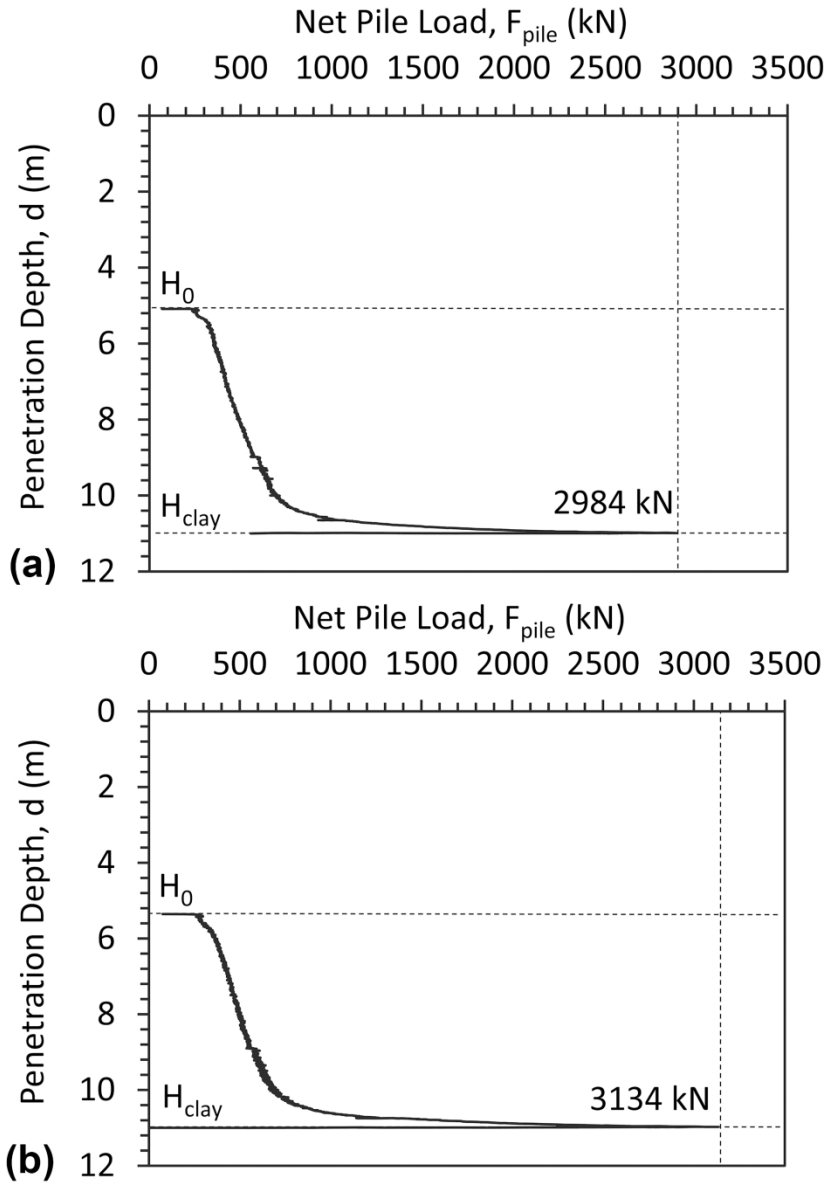

FIG. 13. Load-penetration curves of the piles during room-temperature installation to the target depth (with maximum load shown as a vertical line): (a) Unheated pile; (b) Heated pile

88x128mm (600 x 600 DPI)

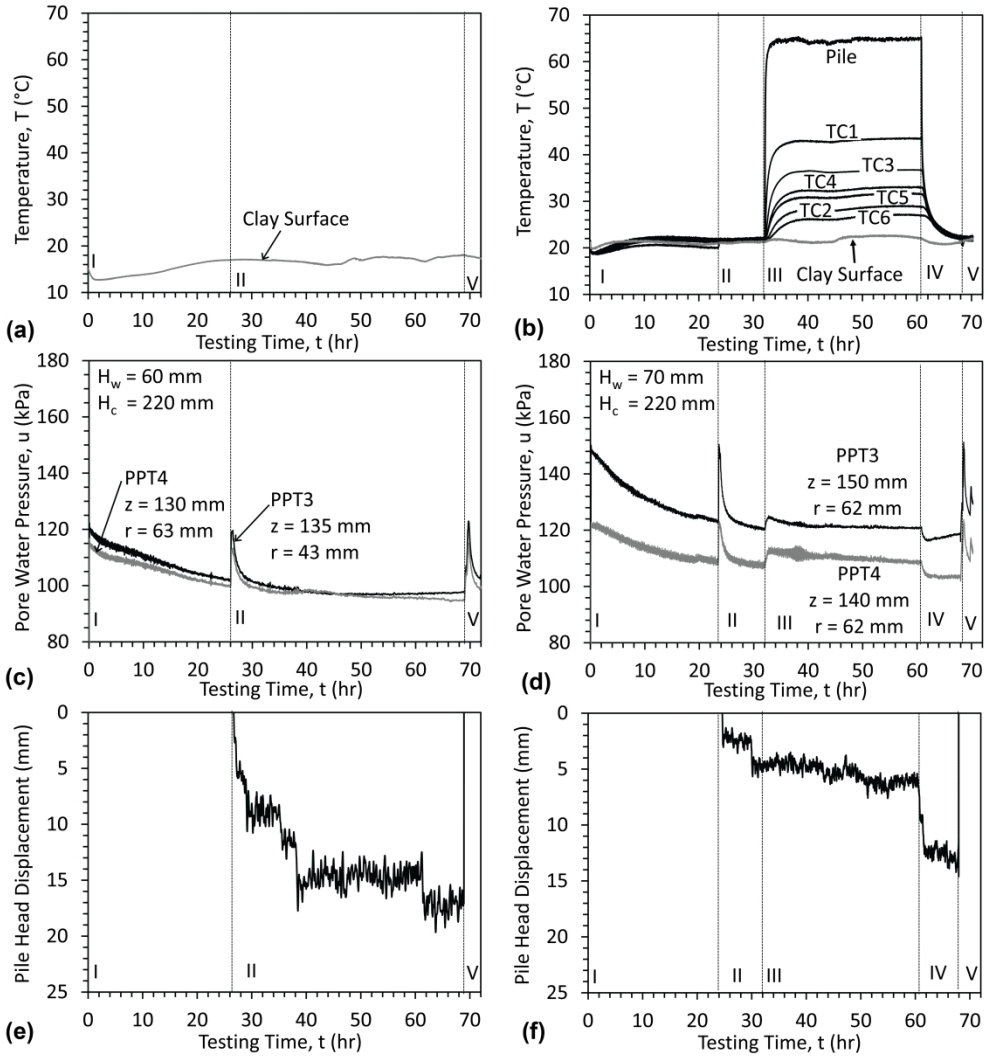

FIG. 14. Testing time series results for centrifuge tests, with time in model scale and other variables in prototype scale: (a) Temperature at clay surface (unheated pile); (b) Temperature of soil at different radii (heated pile); (c) Pore water pressure at different radii (unheated pile); (d) Pore water pressure at different radii (heated pile); (e) Pile head displacement (unheated pile); (f) Pile head displacement (heated pile).

177x187mm (600 x 600 DPI)

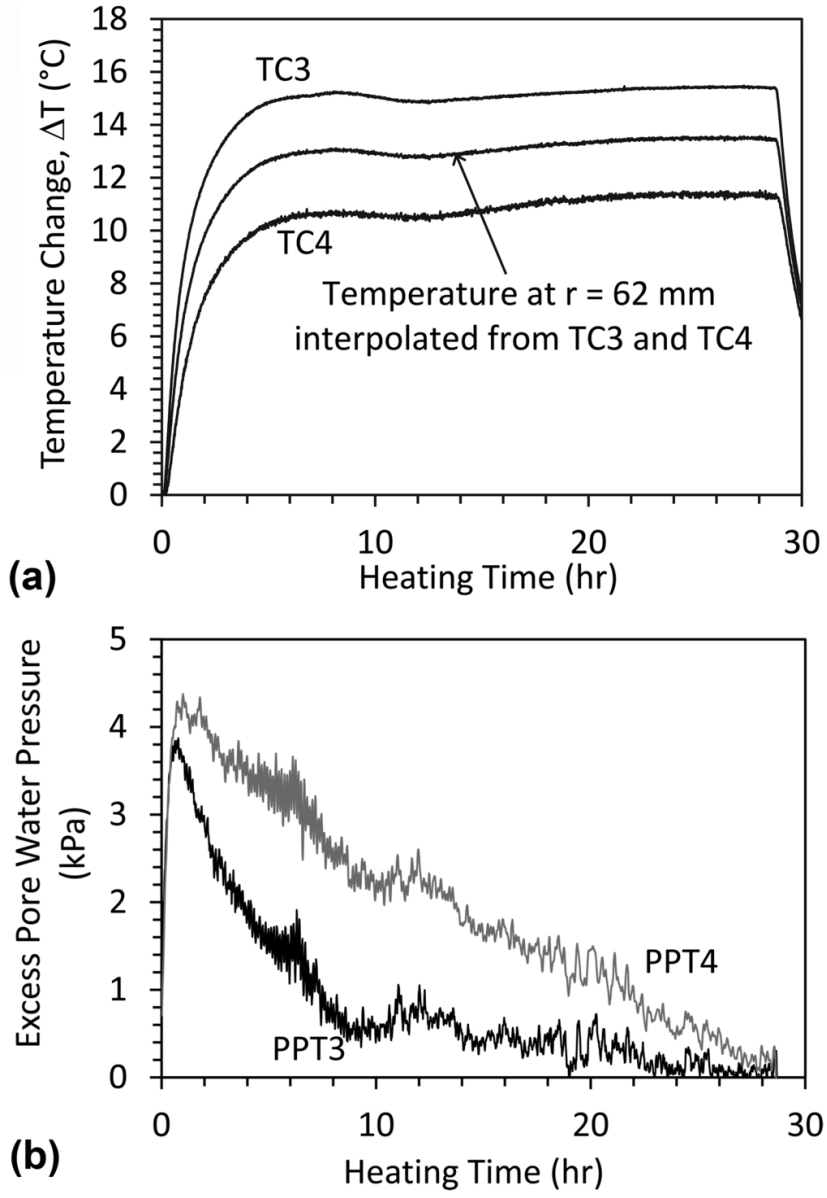

FIG. 15. Further interpretation of time series from heated pile test, with time in model scale: (a) Temperature change vs. heating time estimated at a radius representative of both pore water pressure transducer locations; (b) Thermally induced excess pore water pressure vs. heating time.

88x124mm (300 x 300 DPI)

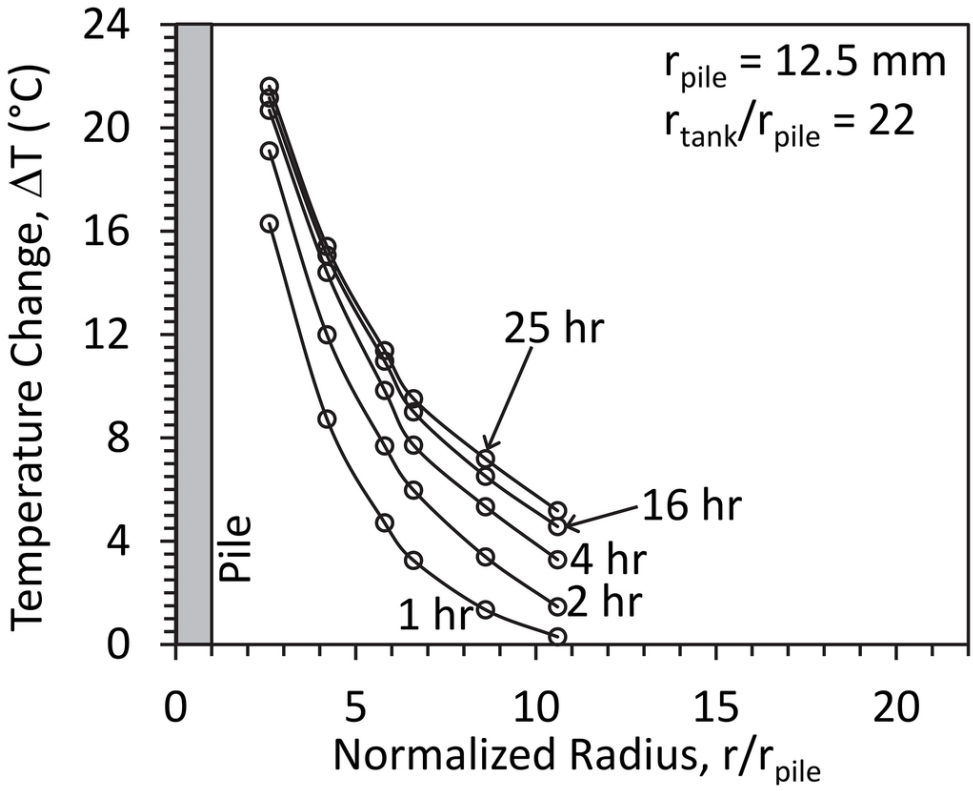

FIG. 16. Radial distribution in soil temperature change after different heating times.

88x72mm (300 x 300 DPI)

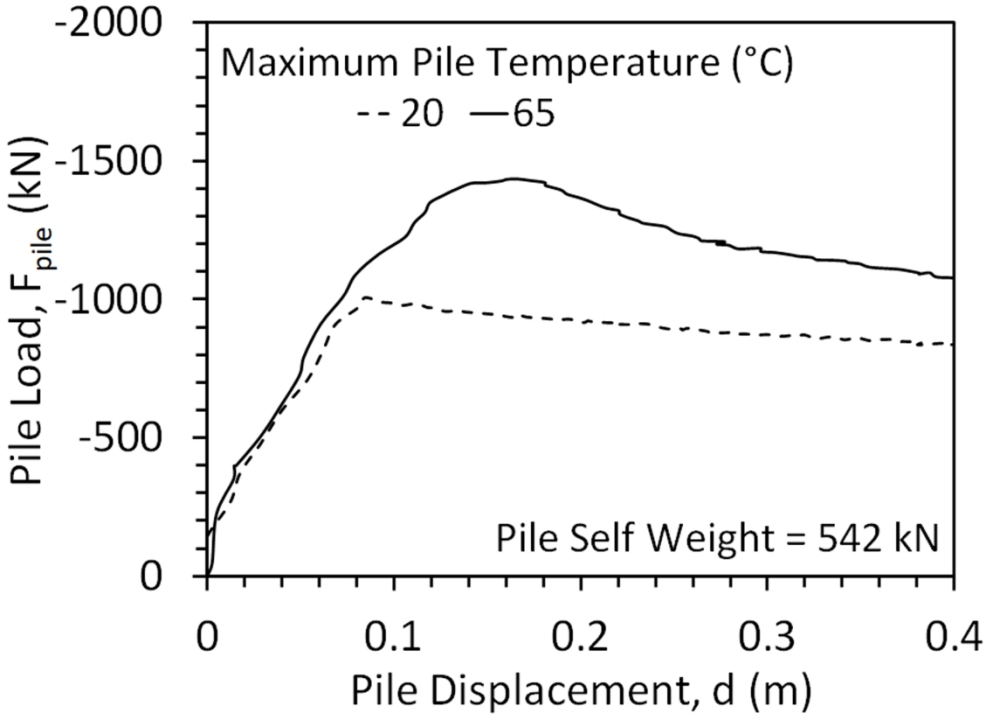

FIG. 17. Pullout load displacement curves for unheated and heated piles.

88x64mm (600 x 600 DPI)

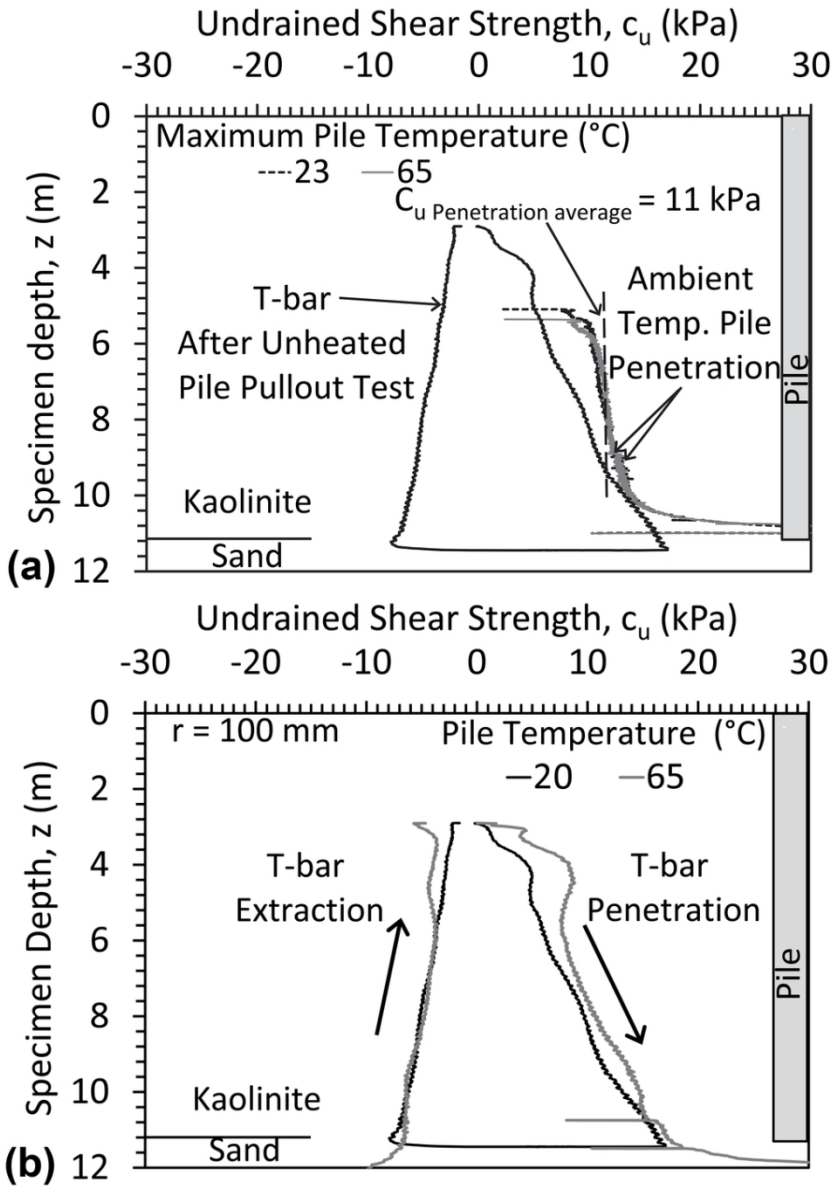

FIG. 18. Undrained shear strength profiles (positive values used to denote the undrained shear strength during insertion and negative values denote the undrained shear strength during extraction): (a) T-bar measurements for tests on unheated and heated piles; (b) Comparison of T-bar measurements at room temperature with those inferred from pile installation with temperatures to differentiate the two piles.

88x123mm (300 x 300 DPI)

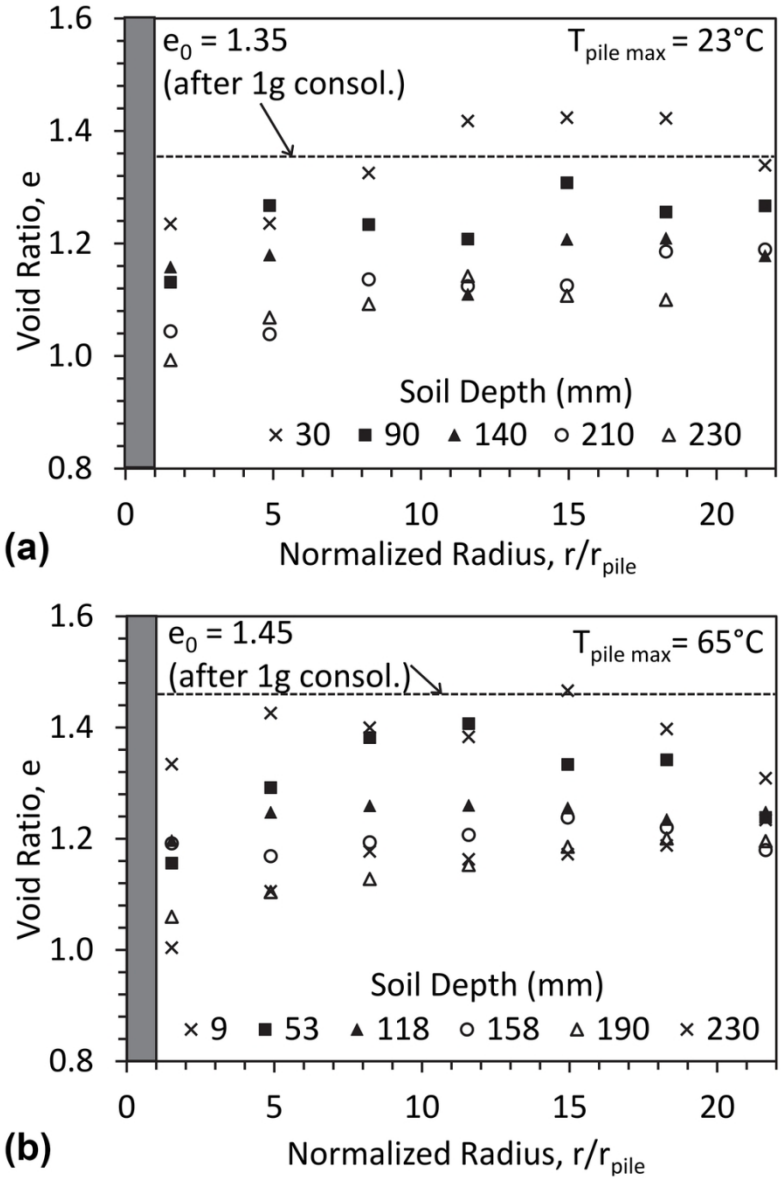

FIG. 19. Post-test measurements of void ratio as a function of depth and radial distance from the center of the pile (model-scale dimensions); (a) Unheated pile; (b) Heated pile.

88x132mm (300 x 300 DPI)